Chinese Chemical Letters 36 (2025) 110035

Contents lists available at ScienceDirect

Chinese Chemical Letters

journal homepage: www.elsevier.com/locate/cclet

Recovering Ag^+ with nano-MOF-303 to form Ag/AgCl/MOF-303 photocatalyst: The role of stored Cl^- ions

Ming-Yi Sun, Lu Zhang, Ya Li, Chong-Chen Wang*, Peng Wang, Xueying Ren, Xiao-Hong Yi

Beijing Key Laboratory of Functional Materials for Building Structure and Environment Remediation, School of Environment and Energy Engineering, Beijing University of Civil Engineering and Architecture, Beijing 100044, China

ARTICLE INFO

Article history:
Received 5 February 2024
Revised 25 April 2024
Accepted 20 May 2024
Available online 21 May 2024

Keywords:
MOF-303
Silver ions
Resource recovery
Photocatalyst
Mechanism

ABSTRACT

The nano-MOF-303 synthesized by microwave method exhibited efficient adsorption capacity (232 mg/g) toward Ag^+, in which the adsorption behaviors were fitted by the *pseudo*-second-order kinetic and the Freundlich isotherm model. The outstanding Ag^+ sorption ability of nano-MOF-303 could be contributed to electrostatic interactions, weak coordination interaction of Ag-N, and AgCl precipitates originating from the stored Cl^- in nano-MOF-303. Besides the adsorbent regeneration, the formed Ag/AgCl onto nano-MOF-303 could produce Ag/AgCl/MOF-303 as a photocatalyst for sulfamethoxazole degradation under visible light. In this work, both the adsorption and photocatalysis mechanisms were clarified, which might provide insight to develop more effective adsorbents for mining the critical resource from the wastewater.

As a precious metal, silver is widely used in various fields including but not limited to photographic industry [1,2], electronic applications [3], and even consumer goods [4]. Considering the outstanding antibacterial ability, in 2020, more than 100,000 tons silver nanoparticle was used in the textile for socks, undergarments and wound dressings [5]. Although trace silver could exhibit effective antibacterial ability, it was reported that high concentrations of silver in the water pose a great threat to the environment [6,7]. It was necessary to remove and recover Ag from the aqueous waste streams from both environment sustainability and resource recycling. Adsorption is deemed as a preferential method to remove and recover Ag^+ due to that it can concentrate the low or even trace concentration of Ag^+ to facilitate the subsequent reuse. In our previous work, we utilized NH_2-MIL-125(Ti) to remove and recover the Ag^+ from the simulated wastewater, in which the saturated NH_2-MIL-125(Ti) could be transferred into Ag/C/TiO_2 photocatalyst under high temperature [8]. The above-mentioned work practiced the 3Rs strategy (reduce, recycle and reuse) and achieved triple objectives of eliminating pollution, recovering resource, and reusing resource [9].

Nano-MOF-303, as an environmentally friendly Al-MOF, demonstrated some characteristics like porous structure, large surface area, outstanding thermal stability and chemical stability [10]. Nano-MOF-303 is constructed from Al^{3+} and 1-*H*-pyrazole-3,5-dicarboxylate (PZDC) linkers, in which two exposed nitrogen atoms in the pyrazole ring might interact with the metal ions. According to the previous report [11], there were generally four ways like solvothermal, reflux, vessel and microwave-assisted ones to synthesize MOF-303. Traditional synthesis approaches can achieve stable textural properties, morphology and affinity for adsorption, which suffered from long reaction time, high temperature and pressure. Fortunately, the microwave assisted method demonstrated some advantages including short reaction time (within 30 min), high yield and easy crystal nucleation. In this work, we utilized the massive Cl^- anions from the $AlCl_3$ precursor left in the framework of nano-MOF-303 to enhance the adsorption capacity *via* the formation of AgCl precipitates and produce Ag/AgCl/MOF-303 composite as a potential photocatalyst (Fig. 1a) [12]. For example, Zhang *et al.* [13] fabricated a ternary Ag/AgCl/ NH_2-UiO-66 photocatalyst using chemical reagents to achieve effective photocatalytic Cr(VI) reduction, in which the Cr(VI) reduction performance was superior to the pristine NH_2-UiO-66 due to the boosted separation of photo-induced electrons and holes.

The information of the chemicals and analytic methods was provided in Texts S1 and S2 (Supporting information).

In this study, high throughput nano-MOF-303(Al) was synthesized by a microwaved-assisted approach (Text S3 in Supporting information) [11]. The PXRD patterns (Fig. 1b) of the synthesized nano-MOF-303 particles were well matched with the single crystal data (CCDC #2078717), indicating nano-MOF was successfully synthesized with high purity. The specific surface area (1338.8 m^2/g) and pore volume (0.7993 cm^3/g) of the as-prepared nano-MOF were comparable to those reported in the previous reports (Fig.

* Corresponding author.
E-mail address: wangchongchen@bucea.edu.cn (C.-C. Wang).

https://doi.org/10.1016/j.cclet.2024.110035
1001-8417/

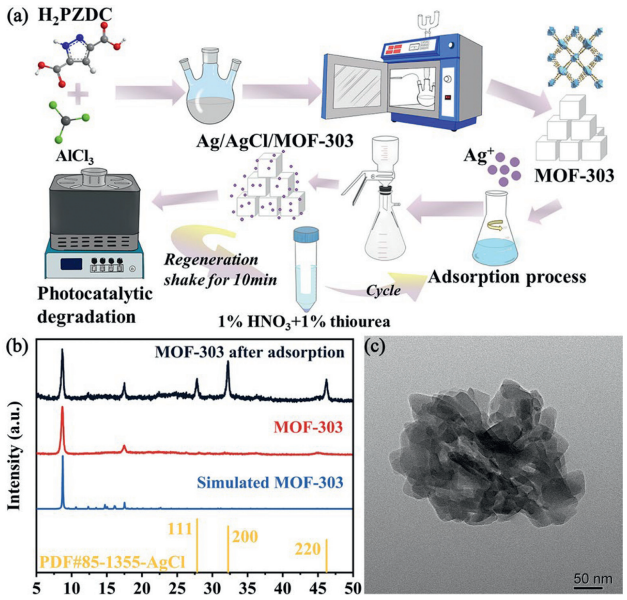

Fig. 1. (a) Synthetic illustration for the nano-MOF-303 preparation and the reuse strategy. (b) The PXRD patterns of nano-MOF-303 before and after adsorption. (c) The HRTEM images of nano-MOF-303.

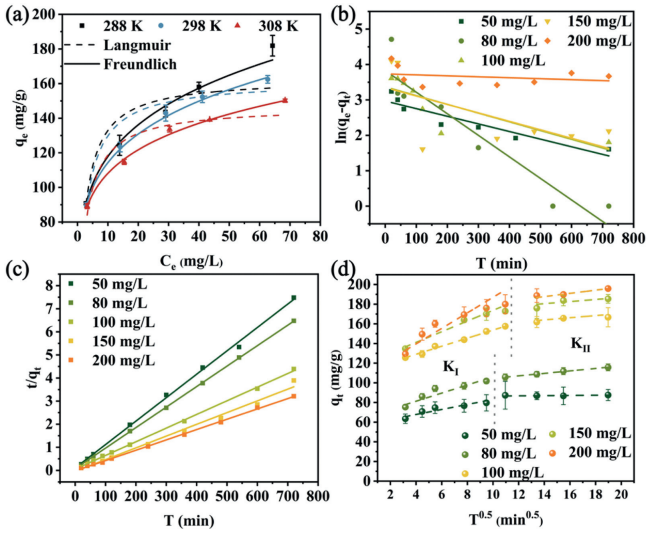

Fig. 2. (a) The adsorption isotherms model of nano-MOF-303 for Ag^+ adsorption under different temperatures. (b) *pseudo*-first-order and (c) *pseudo*-second-order kinetics models for sorption process of Ag^+ on nano-MOF-303. (d) The intra-particle diffusion models for adsorption process. Experimental conditions: sorbent dosage = 0.2 mg/L, $[Ag^+]_0$ = 20 mg/L, initial pH 5.6, T = 25 °C.

S1 in Supporting information) [14]. The high-resolution transmission electron microscope (HRTEM) image (Fig. 1c and Fig. S2 in Supporting information) revealed that the nano-MOF exhibited irregular particles with the size of 50 nm [15], which was smaller than those synthesized by the solvothermal method (100–500 nm). This may be due to the rapid synthesis kinetics of the microwave method shorten the time of particle growth.

The adsorption experiment (Text S4 in Supporting information) results revealed that the as-prepared nano-MOF-303 displayed excellent adsorption ability toward Ag^+ cations with maximum adsorption capacity of 232 mg/g, which surpassed the other previous adsorbents (Table S1 in Supporting information). Three isotherm models like Langmuir and Freundlich were employed to understand how the Ag^+ ions interact with the nano-MOF-303 (the detailed calculation can be found in Support information). As depicted in Fig. 2a and Table S2 (Supporting information), the higher fitting correlation coefficients R^2 (0.9953-0.9966) of the Freundlich model revealed that the uptake of Ag^+ by nano-MOF-303 was mainly a multilayer adsorption process [16]. The value of $1/n < 1$ represented that the adsorption energy decreased as the surface concentration increased [17]. The q_{max} value estimated by the Freundlich model decreased with increasing temperature, confirming that the adsorption of Ag^+ ions over nano-MOF-303 was exothermic. The K_F decreased with the temperature increasing, further verifying that it is favorable for the adsorption of Ag^+ on the adsorbent at low temperatures. To ulteriorly understand the adsorption, the thermodynamic parameters including standard enthalpy change (ΔH^0, kJ/mol), standard entropy change (ΔS^0, J mol^{-1} K^{-1}) as well as standard Gibbs free energy (ΔG^0, kJ/mol) were calculated by formula (Supporting information), based on the results obtained from the adsorption isotherm. The exothermic sorption process was affirmed by the negative ΔH^0 (−45.64 kJ/mol) as presented in Table S3 (Supporting information). From the experimental results, it can be seen that the adsorption process of nano-MOF-303 toward Ag^+ was inhibited by the increase in temperature. The positive ΔS^0 (35.51 J mol^{-1} K^{-1}) indicated that the high affinity between nano-MOF-303 and Ag^+ ions resulted in increased randomness. The Gibbs free energy variation from −10.27 kJ/mol to −10.98 kJ/mol in the temperature range of 293 K to 303 K further verified that the absorption of Ag^+ on nano-MOF-303 was thermodynamically spontaneous.

The adsorption kinetics models fitting results of Ag^+ on nano-MOF-303 were shown in Figs. 2b and c and Table S4 (Supporting information). It was obvious that the adsorption kinetics of nano-MOF-303 followed the *pseudo*-second-order model. Besides, the predicted equilibrium adsorption capacity (223 mg/g) was consistent with the actual experimental adsorption capacity data (232 mg/g). The high fit proved that the adsorption process was mainly chemisorption.

The intra-particle diffusion model was always applied to ascertained whether the rate-limiting steps determined the intraparticle diffusion. Fig. 2d exhibited that both intraparticle and extra particle diffusion were responsible for controlling the adsorption rate because the linear fit of the intraparticle diffusion model did not pass through the origin. In the process of mass transfer of silver ions in solution, three main stages occurred. The first step showed that Ag ions migrated by membrane diffusion to the nano-MOF-303's outer surface, which was followed by intra-particle diffusion from the boundary layer to the adsorbent's pores. In the last stage, silver ions were gradually adsorbed to the active sites to realize the adsorption-desorption equilibrium. Table S4 (Supporting information) demonstrated the intra-particle diffusion constants K_I and K_{II} for adsorption's first and second stages. Since K_I was greater than K_{II}, indicating that Ag^+ ions were rapidly diffused at the beginning of adsorption. Then, they entered the slow adsorption phase, when Ag^+ occupied the majority of the adsorption sites of nano-MOF-303 surface, in which the increased ion competitions and decreased the mass transfer driving force in turn slowed down the adsorption rate [18]. The experimental results of the intra-particle diffusion model showed that the adsorption process of Ag^+ on nano-MOF-303 was controlled by both film diffusion and intra-particle diffusion.

Aqueous solution pH was an important parameter in the adsorption process, owing to the hydronium ions could influence the adsorbent surface charge and adsorbate state of existence. On the other hand, considering that at higher pH values, precipitates of silver hydroxide would be formed [8]. The influence of pH on the Ag^+ adsorption of nano-MOF-303 was analyzed by varying the pH values between 2.0 and 5.0 (Fig. 3a). It was observed that the ad-

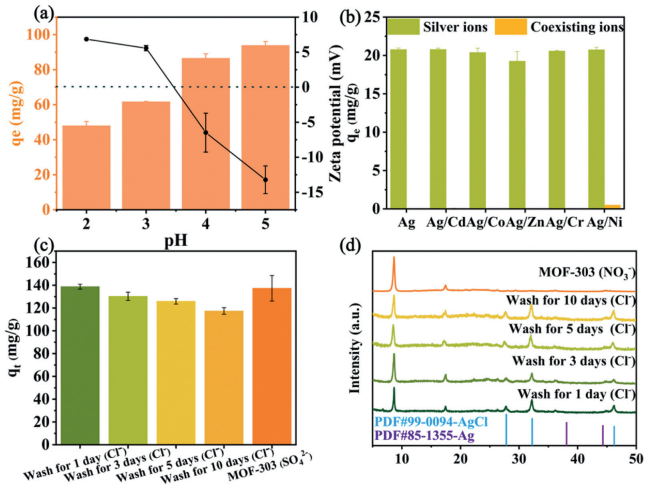

Fig. 3. (a) Effect of pH on adsorbed amount of Ag^+ ($C_0 = 50$ mg/L) and zeta potential of nano-MOF-303 at different pH value. (b) Effects of interfering ions on the Ag^+ capture. $[Cd^{2+}]_0$, $[Co^{2+}]_0$, $[Zn^{2+}]_0$, $[Cr^{3+}]_0$, $[Ni^{2+}]_0 = 1$ mg/L, $[Ag^+]_0 = 5$ mg/L. (c) The effect of Cl^- on the adsorption process. $[Ag^+]_0 = 80$ mg/L. sorbent dosage = 0.2 mg/L. (d) The PXRD of nano-MOF-303 after adsorption with different degrees of washing.

sorption capacities increase slightly as the initial pH of the solution increased. Based on the zeta potential, the isoelectric point (zero value of zeta potential) of nano-MOF-303 occurred at pH 3.5. The nano-MOF-303 adsorbent exhibited negative surface charge at pH > 3.5 (Fig. 3a), which facilitated the boosted interactions between negatively charged nano-MOF-303 and positively charged Ag^+ cations [19].

In order to study interference of other competing ions, different cations like Ni^{2+}, Zn^{2+}, Cd^{2+}, Cr^{3+}, and Co^{2+} were added to the Ag^+ solution to simulate silver plating wastewater samples. Nano-MOF-303 exhibits high selectivity towards Ag^+ (Fig. 3b), indicating that it can be potentially applied as an adsorbent to mine the Ag^+ from some specific wastewater containing silver ions. Moreover, nano-MOF-303 synthesized by microwave method exhibited better adsorption capacity (117 mg/g) than those synthesized by solvothermal method (90 mg/g). It could be attributed to that the smaller particle size that increased the contact area and active sites of the adsorbent to interact with the silver ions (Fig. S3 in Supporting information). Some stored Cl^- anions may be washing off from the nano-MOF-303 (Fig. S4 in Supporting information), possibly leading to the decreased adsorption capacity. The results affirmed that the adsorption capacities decreased from 127.64 mg/g of pristine nano-MOF-303 to 119.45 mg/g of sample being washed for 10 d and could maintain their stability (Figs. 3c and d), implying that the stored Cl^- in the framework of nano-MOF-303 left from the reaction precursor $AlCl_3$ could further enhance the capture ability toward Ag^+ due to the formation of AgCl precipitates. While, the adsorbent nano-MOF-303 synthesized from precursor $Al(NO_3)_3$ exhibited poorly adsorption capacity (92.96 mg/g), which further authenticated the stored Cl^- played an irreplaceable role in recovering Ag^+.

Several adsorption interactions could potentially be involved in the adsorption of nano-MOF-303 toward Ag^+. The PXRD patterns of fresh and used nano-MOF-303 were measured (Fig. 1a). It was seen that the new peaks of 2θ being 27.82°, 32.24° and 46.24° attributed to (111), (200) and (220) typical crystal facets of AgCl [20]. The result revealed that, along with the electrostatic interaction between nano-MOF-303 and Ag^+, the chemical precipitation of AgCl enhanced the adsorption. In Figs. 4a and b, the high-resolution TEM (HRTEM) revealed that the presence of central atom (Al) and nano-MOF-303 particles were doped with some Ag/AgCl crystal particles, which can be demonstrated by the EDS

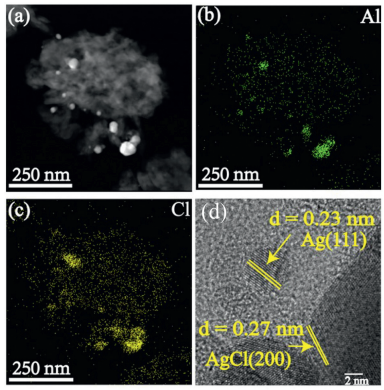

Fig. 4. (a) STEM-HAADF images of Ag/AgCl/MOF-303. (b, c) The EDS mapping of nano-MOF-303 after adsorption. (d) High-resolution TEM of Ag/AgCl/MOF-303.

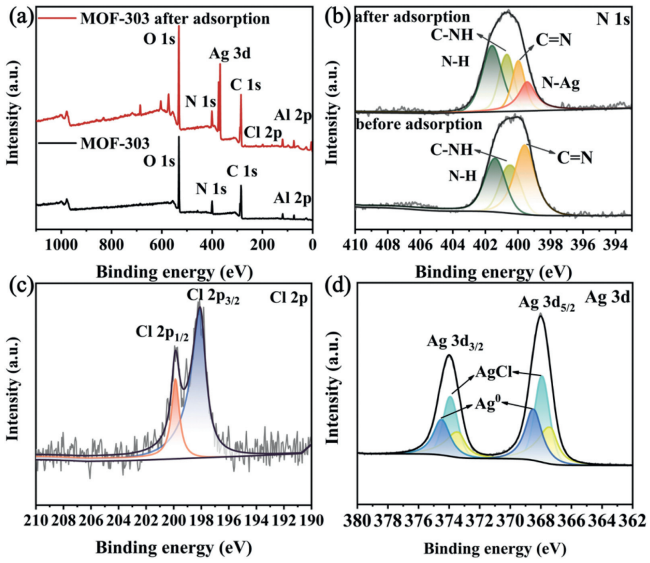

Fig. 5. The XPS spectra of nano-MOF-303 and Ag/AgCl/MOF-303, (a) Survey, (b) N 1s, (c) Cl 2p (d) Ag 3d.

determination (Fig. 4c) and the lattice of $d = 0.27$ nm (facet (200) of AgCl) and $d = 0.23$ nm (facet (111) of Ag^0) [8,21] in HRTEM image (Fig. 4d).

The X-ray photoelectron spectroscopy (XPS) spectra of the fresh and used nano-MOF-303 could further affirm the formation of Ag/AgCl during the adsorption process (Fig. 5a). The peaks at 285.17, 368.20, 400.84, 74.92, and 532.24 eV were assigned to C 1s, Ag 3d, N 1s, Al 2p, and O 1s, respectively. And the representative peaks of 368.20 eV verified that silver cations were adsorbed into the nano-MOF-303. As depicted in Fig. 5b, XPS apectra of N 1s could be divided into C=N (399.58 eV), C-NH (400.45 eV), and N-H (401.40 eV) species [22,23]. After adsorbing Ag^+, the peak of C=N at 399.58 eV weakened obviously, and a new peak belonging to Ag-N (399.44 eV) was appeared, indicating that the nitrogen atoms in C=N could interact with Ag^+ to form Ag-N bond. The spectra of Cl 2p (Fig. 5c) indicated that the binding energies of 199.87 eV and 198.09 eV could be assigned to Cl $2p_{1/2}$ and Cl $2p_{3/2}$ [24]. As shown in Fig. 5d, the peaks at 373.41 eV and 367.38 eV can be attributed to AgCl, whereas the peaks at 374.48 eV and 368.48 eV can be attributed to Ag^0 [21,25,26]. Combined with the above experimental and characterization results, it could be included that electrostatic interaction, Ag-N bond and AgCl precipitate primarily contributed to the boosted adsorption ability of nano-MOF-303 toward Ag^+.

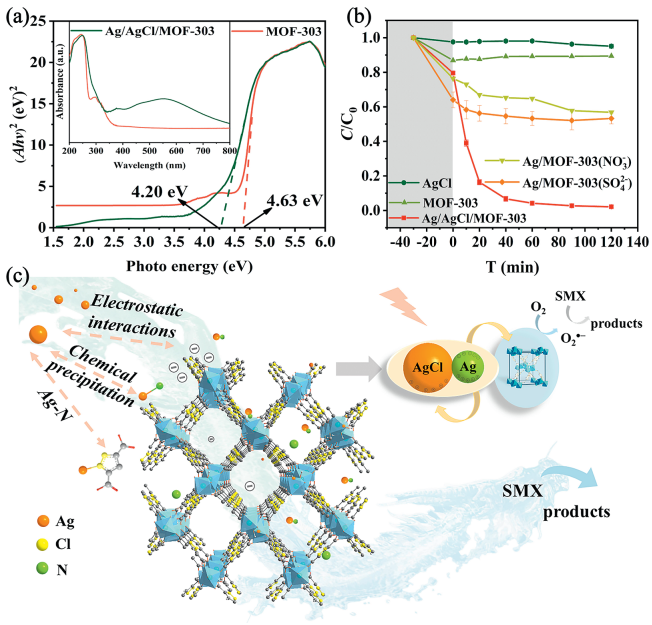

Fig. 6. (a) UV–vis DRS and (inset) E_g plots of nano-MOF-303 and corresponding Ag/AgCl/MOF-303. (b) The SMX degradation under different photocatalysts (Experimental conditions: dosage = 0.2 mg/L, initial pH 5.9, $[SMX]_0 = 5$ mg/L). (c) Adsorption mechanism of nano-MOF-303 for Ag^+ and photocatalysis mechanism of Ag/AgCl/MOF-303.

The recyclability of nano-MOF-303 was examined by regeneration *via* several adsorption-desorption cycles, in which NaOH, HCl, HNO_3, and thiourea were employed as desorbing agents. It was found that the mixture of 1% HNO_3 and 1% thiourea solutions exhibited the best desorption ability. As shown in Fig. S5a (Supporting information), the adsorbed Ag^+ into nano-MOF-303 could be desorbed within 10 min, in which 66% Ag^+ could be desorbed in the second cycle. Subsequently, the PXRD patterns of the desorbed nano-MOF-303 agreed well with the pristine nano-MOF-303, in which the typical peaks of AgCl evidently disappeared (Fig. S5b in Supporting information). After three cycles of adsorption-desorption, nano-MOF-303 maintained stable adsorption capacity and phase stability, implying that nano-MOF-303 demonstrated high chemical stable and satisfactory reusability.

Apart from the desorption for reusing nano-MOF-303 as adsorbent to remove and recover the Ag^+ from the aqueous solution, the formation of Ag/AgCl onto the nano-MOF-303 might accomplish the as-formed Ag/AgCl/MOF-303 acting as effective photocatalyst. As illustrated in Fig. 6a, the UV–vis DRS revealed that the used nano-MOF-303 could absorb the visible light in the wavelength range from 400 nm to 600 nm, indicating that the introduction of Ag/AgCl achieved the as-formed Ag/AgCl/MOF-303 could be irradiated by visible light. The charge carrier transfer and recombination were further affirmed by electrochemical impedance spectroscopy (EIS) determination, in which the Ag/AgCl/MOF-303 displayed smaller Nyquist arc radius (Fig. S6a). The Ag nanoparticles on the surface of the nano-MOF-303 with the strong surface plasmon resonance (SPR) effect dramatically improved the ability to absorb visible light, implying that the Ag/AgCl/MOF-303 displayed better electrical conductivity and smaller radius [27].

As a model pollutant, the sulfamethoxazole (SMX) was selected to assess the photocatalytic activity of Ag/AgCl/MOF-303 under the irradiation of low power LED visible light (25 W) (Text S5 in Supporting information) [28]. The pristine nano-MOF-303 exhibited weak adsorption and degradation activity toward SMX. In addition, it was observed that less than 30% SMX was adsorbed onto Ag/AgCl/MOF-303 under dark conditions for 30 min, possibly due to the Ag-S bond generation. As illustrated in Fig. 6b, 99.0% SMX can be degraded by Ag/AgCl/MOF-303 under visible light irradiation for 40 min. As shown in Fig. S6b (Supporting information), to identify the active species during the photocatalysis process, TBA, BQ, EDTA-2Na, and L-histidine (0.2 mmol/L) were utilized to capture $^{\bullet}OH$, $O_2^{\bullet-}$, and e^-, respectively [29]. The addition of TBA and EDTA-2Na exerted little influence on SMX degradation. Conversely, the SMX degradation efficiency extremely declined after introducing BQ, demonstrating that $O_2^{\bullet-}$ might dominate the degradation of SMX over the Ag/AgCl/MOF-303. The SPR effect of Ag^0 could enhance the visible-light absorption ability, and the component of Ag/AgCl could also improve the separation of the photoinduced charge carriers. More photo-induced electrons were utilized to react with O_2 to form $O_2^{\bullet-}$ radicals for SMX degradation. It was concluded that the introduction of Ag/AgCl not only boosted visible light adsorption, but also enhanced the separation of photogenerated electrons and holes (Fig. 6c).

In all, the as-prepared nano-MOF-303 could capture the Ag^+ ions from the wastewater, which could be ascribed to the electrostatic interaction, weak Ag-N coordination bond and the formation of AgCl precipitates resulted from the stored Cl^- ions in the framework of nano-MOF-303. Different from the traditional desorption treatment for re-generation and reuse of adsorbents, an effective Ag/AgCl/MOF-303 photocatalyst was developed to accomplish organics degradation under visible light due to the formation of Ag/AgCl onto nano-MOF-303 during the adsorption process. In our work, the Cl^- stored in the framework can not only synergize with nano-MOF-303 to promote the adsorption process, but also form Ag/AgCl/MOF-303 heterojunction photocatalyst with good photocatalytic performance, which pave an avenue for practical industrial wastewater treatment. This work provided a case of "Reduction of pollution and carbon emissions" to mine the critical resource and eliminated the pollutants from wastewater for sustainable development.

Declaration of competing interest

The authors declare that they have no known competing financial interests or personal relationships that could have appeared to influence the work reported in this paper.

CRediT authorship contribution statement

Ming-Yi Sun: Data curation, Investigation, Visualization, Writing – original draft. **Lu Zhang:** Investigation, Methodology. **Ya Li:** Investigation, Methodology. **Chong-Chen Wang:** Conceptualization, Funding acquisition, Project administration, Supervision, Writing – review & editing. **Peng Wang:** Resources. **Xueying Ren:** Methodology, Resources. **Xiao-Hong Yi:** Methodology, Resources.

Acknowledgments

This work was supported by National Natural Science Foundation of China (Nos. 22176012, 51878023), BUCEA Post Graduate Innovation Project (No. PG2023057) and BUCEA Doctor Graduate Scientific Research Ability Improvement Project (No. DG2024022).

Supplementary materials

Supplementary material associated with this article can be found, in the online version, at doi:10.1016/j.cclet.2024.110035.

References

[1] S. Singha, D. Kim, H. Seo, et al., Chem. Soc. Rev. 44 (2015) 4367–4399.
[2] L. Zhang, Y.H. Li, L.H. Meng, et al., Sep. Purif. Technol. 341 (2024) 126928.

[3] F. Peng, W. Zhu, Y. Fang, et al., ACS Appl. Mater. Interfaces 15 (2023) 4284–4293.
[4] T. Nawaz, S. Sengupta, Sep. Purif. Technol. 176 (2017) 145–158.
[5] T. Nawaz, S. Sengupta, ACS Sustain. Chem. Eng. 6 (2018) 600–608.
[6] D. Kou, W. Ma, S. Zhang, Adv. Funct. Mater. 31 (2021) 2007032.
[7] R. Li, T. Gao, W. Qiu, et al., Nano Res. 17 (2024) 2438–2443.
[8] X. Ren, C.C. Wang, Y. Li, et al., Chem. Eng. J. 442 (2022) 136306.
[9] P. Li, L. Liao, Z. Fang, et al., Proc. Nat. Acad. Sci. U. S. A. 120 (2023) e2305489120.
[10] N. Hanikel, X. Pei, S. Chheda, et al., Science 374 (2021) 454–459.
[11] Z. Zheng, H.L. Nguyen, N. Hanikel, et al., Nat. Protocol. 18 (2023) 136–156.
[12] Y. Fan, W. Zhang, K. He, et al., Appl. Surf. Sci. 591 (2022) 153115.
[13] Z. Zhang, S. Wang, M. Bao, et al., J. Colloid Interface Sci. 555 (2019) 342–351.
[14] H. Wang, Z. Shi, J. Yang, et al., Angew. Chem. Int. Ed. 60 (2021) 3417–3421.
[15] M. Li, X. Wang, J. Zhang, et al., Appl. Surf. Sci. 619 (2023) 156819.
[16] T. Wang, J. He, J. Lu, et al., Chin. Chem. Lett. 33 (2022) 3585–3593.
[17] C. Xinyu, H. Md Faysal, D. Chengyu, et al., Chemosphere 307 (2022) 135545.
[18] Z. Wang, X. Gu, X. Zhang, et al., Sci. Total Environ. 901 (2023) 166312.
[19] X.D. Du, C.C. Wang, J.G. Liu, et al., J. Colloid Interface Sci. 506 (2017) 437–441.
[20] B. Li, F. Mumtaz, X. Li, et al., Chem. Eng. J. 470 (2023) 144369.
[21] J.Y. Park, I. Lee, J. Ham, et al., Nat. Commun. 8 (2017) 15650.
[22] B. Liu, L. Pei, X. Zhao, et al., Chem. Eng. J. 410 (2021) 128431.
[23] H. Li, P. Li, Y. Guo, et al., Anal. Chem. 96 (2024) 997–1002.
[24] N. Liu, J. Zhang, Y. Wang, et al., Nanomaterials 12 (2022) 1946.
[25] S.F. Yang, C.G. Niu, D.W. Huang, et al., Environ. Sci. Nano 4 (2017) 585–595.
[26] P. Wang, B. Huang, Z. Lou, et al., Chem. Eur. J. 16 (2010) 538–544.
[27] L. Wang, J. Zhang, Y. Li, et al., Appl. Catal. B: Environ. 336 (2023) 122921.
[28] Y. Ni, C. Zhou, M. Xing, et al., Green Energy Environ. 9 (2024) 417–434.
[29] Y. Zhou, Y. He, M. Gao, et al., Chin. Chem. Lett. 35 (2024) 108690.